

Towards Automatic Localization and Anatomical Labeling of Intracranial Depth Electrodes in Brain Images

Chester Huynh¹, Adam Li¹, Jorge Gonzalez-Martinez², and Sridevi V. Sarma¹

Abstract—Patients with focal medically refractory epilepsy (MRE) suffer from recurrent seizures that cannot be controlled with anti-epileptic drugs. These patients are candidates for surgical interventions in hopes of treating the epileptogenic zone, a cortical region indispensable to seizure generation. Techniques used by clinicians in pre-surgical planning include implantation of stereoelectro-encephalography (SEEG) electrodes for high spatial and temporal resolution. The localization and anatomical labeling of SEEG electrode contacts are essential, but time-consuming tasks often done manually by trained clinicians. We propose a threshold clustering-based algorithm for semi-automatically localizing and anatomically labeling SEEG contacts, using a computed tomography brain scan, a brain-mask, and positions of the entry and exit points for each electrode. The centroids of each outputted cluster are computed and compared against the positions of the manually labeled contacts. These centroids are then anatomically labeled using Destrieux and Desikan-Killany brain parcellation atlases. Our algorithm was applied on three MRE patients who underwent surgical treatment. The largest average error between the computed centroids and manually labeled contacts was 0.493 mm. The algorithm was completed within minutes for each patient without the need for trained experts.

I. INTRODUCTION

Focal epilepsy is a neurological disorder that affects more than 60 million people worldwide [1]. Approximately 30% of these cases are classified as medically refractory epilepsy (MRE), wherein patients suffer from recurrent seizures that cannot be controlled by anti-epileptic drugs [1], [2], [3], [4], [5]. Patients with MRE are considered candidates for surgical treatment in hopes of removing the epileptogenic zone (EZ) [6], [7], a region of the cerebral cortex found to be indispensable for seizure generation. Preserving eloquent cortex is the other primary goal of epilepsy surgery. [8]. Clinicians utilize intracranial EEG (iEEG) recordings, which include electrocorticography (ECoG) and stereo-electro-encephalography (SEEG), to obtain high intracortical spatial and temporal resolution measurements, complementing their analyses through noninvasive recording methods, such as functional magnetic resonance imaging and magnetoencephalography [7], [9], [10].

Correct interpretation of iEEG recordings relies on precise knowledge of the anatomical location of each electrode [6], [11], [12]. However, the localization of iEEG electrodes in post-implantation images remains a time-consuming procedure as identification is often done manually by trained clinicians, requiring advanced 3D visualization tools and

detailed knowledge of MRI-based neuroanatomy to minimize errors [5], [11], [12]. The manual localization process is also prone to operator errors, and as such, has motivated the development of methods to automate the localization procedure.

Previous studies have proposed semi-automatic or automatic segmentation algorithms for both ECoG subdural grids and SEEG depth electrodes that provide anatomical labeling by use of brain atlases, which map brain image voxels to anatomical labels [13], [14]. These approaches tend to either be optimized for ECoG or have lower localization accuracy for depth electrodes used in SEEG monitoring. Arnulfo et al. [6] developed a threshold-based segmentation algorithm for localizing SEEG depth electrodes in computed tomography (CT) images, achieving errors of $0.5 \text{ mm} \pm 0.06 \text{ mm}$ across 12 subjects. Despite high localization accuracy, the algorithm requires an input of electrode size and spacing, which are not always available for each patient, limiting the flexibility of the approach [6]. The Curry Neuroimaging Suite, on the other hand, offers a high-quality software for automatic localization and anatomical labeling of depth electrodes, but is a costly option for the task [15].

While there exist algorithmic approaches that can localize various types of iEEG electrode arrays (i.e. ECoG), there are few methods that are optimized solely for the localization of SEEG depth electrodes that are affordable, open-source, accurate, and require minimal user input. We propose a semi-automatic approach for segmenting and labeling SEEG depth electrodes in CT scans using a threshold-based approach and brain parcellation atlases that requires only two manually labeled contacts per SEEG electrode. The algorithm relies on the positions of the bounding (innermost and outermost) contacts along each electrode. It can take in a corresponding brain-mask that strips the skull in the CT image as well, which can be derived from T1 MRI images via FreeSurfer. The algorithm provides an interpretable approach that reduces the need for trained clinicians in the localization procedure. Further, by segmenting entire point clouds associated to each contact, we can robustly assign anatomical labeling to each contact. We implemented the proposed algorithm in Python and is open to contributions at: https://github.com/adam2392/neuroimg_pipeline.

II. METHODS

A. Data Acquisition

In this study, we perform electrode localization for three patients (mean age 30.0 years) that were surgically treated for drug-resistant epilepsy. All patients underwent invasive

¹ Institute for Computational Medicine, Biomedical Engineering, The Johns Hopkins University

² Department of Neurosurgery, University of Pittsburgh

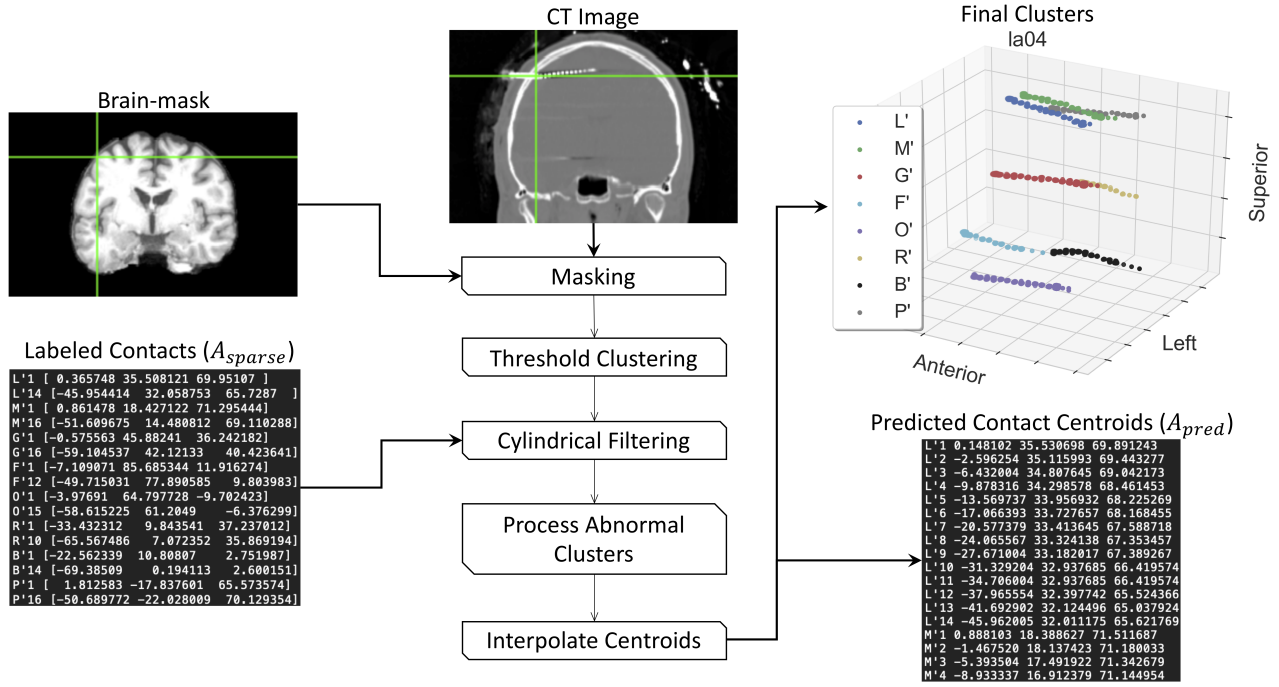


Fig. 1. Sequential schematic for the steps of the electrode localization algorithm. The bold arrows show the inputs (Brain-mask, a minimal set of labeled contacts and CT image) and outputs (predicted contact centroids and the final clusters of contacts per electrode) to the algorithm. Note that besides the labeled entry/exit points of each electrode (A_{sparse}), the algorithm requires no other manual input.

presurgical evaluation using stereo-EEG (SEEG) depth electrode implantations to localize the EZ and delineate eloquent areas. Prior to implantation, T1-weighted MRI was obtained. For each patient, the number and location of implanted electrodes were pre-operatively determined by a pre-implantation hypothesis based on non-invasive data. The decisions of clinicians in determining the need for invasive monitoring and the placement of the depth electrodes were made independently from this work and based solely on clinical necessity. Post-implantation CT images were acquired following surgery to ensure accurate placement and labeling. A 3D reconstruction was produced to visualize electrode placements using the Curry NeuroImaging Suite (NeuroScan, El Paso, TX). The electrode locations were then determined by visual inspection and agreement by at least two clinical experts. T1 and CT data were processed using FreeSurfer, FSL, and Fieldtrip Toolbox [16], [17], [18]. The data used in this study were deidentified and assigned study numbers, e.g. "la04", which were given with no specific ordering. All data were acquired with approval of the Institutional Review Board (IRB). The digitized data used for this study were stored in an IRB-approved database compliant with Health Insurance Portability and Accountability Act (HIPAA) regulations.

B. Electrode Localization

The electrode localization algorithm outputs a set A_{pred} of labeled (x, y, z) -coordinates for each contact along each electrode. The CT image and brain-mask in CT space were provided as input images. The brain-masks were obtained as part of the output from the recon-all FreeSurfer

command. A sparse set A_{sparse} of manually labeled contacts containing coordinates for the bounding (i.e. innermost and outermost) contacts for each electrode was also given as input. The sequence of processing steps performed by the algorithm to localize and label all electrodes is outlined by Figure 1. As a preliminary pre-processing step, the user-specified points A_{sparse} were transformed from (x, y, z) -space to CT space by applying an affine transform.

Masking and normalization. CT voxel intensities that corresponded to electrodes were generally higher than that of tissue voxels, but were similar to that of dense bone within the skull. To strip the skull, the brain-mask was applied to the CT image, though the skull was often not stripped perfectly. The output masked image preserved voxels of the original CT image in which the corresponding voxel in brain-mask was nonzero. The masked CT image was then normalized by dividing each voxel value by a factor of 255, resulting in all voxel values residing in the real interval $[0, 1]$.

Threshold Clustering. A voxel intensity threshold of 0.630 was set to binarize the image. A set A_{thresh} of disjoint clusters from the threshold-masked image were determined and numerically labeled using the `label` method from the scikit-image library. A voxel was considered to be in a cluster if at least one of its neighbors of equal intensity was also in the cluster. Two voxels were considered to be neighbors if they were within two orthogonal hops from each other.

Cylindrical Filtering. Since SEEG depth electrodes are cylindrical in shape, the coordinates for the bounding contacts of each electrode were used to construct cylindrical boundaries with a radius of 4 voxels. These cylindrical

boundaries were used to group the clusters in A_{thresh} to a particular electrode and remove any clusters that did not fall into any of the cylindrical boundaries. Supposing that there are J electrodes, a cluster $C_i \in A_{thresh}$ was assigned to an electrode $j \in \{1, 2, \dots, J\}$ if at least one point in C_i fell within the cylinder formed by the bounding contacts $\vec{p}_{j,1}$ and $\vec{p}_{j,2}$ for electrode j . For a given cluster, each point $\vec{q} \in C_i$ was considered to fall within the cylinder of radius $r = 4$ for electrode j if it satisfied each of the following inequalities

$$(\vec{q} - \vec{p}_{j,1}) \cdot (\vec{p}_{j,2} - \vec{p}_{j,1}) \geq 0 \quad (1)$$

$$(\vec{q} - \vec{p}_{j,1}) \cdot (\vec{p}_{j,2} - \vec{p}_{j,1}) \leq \|\vec{p}_{j,2} - \vec{p}_{j,1}\|_2^2 \quad (2)$$

$$\|\vec{q} - \vec{p}_{j,1}\|_2 - \frac{(\vec{q} - \vec{p}_{j,1}) \cdot (\vec{p}_{j,2} - \vec{p}_{j,1})}{\|\vec{p}_{j,2} - \vec{p}_{j,1}\|_2} \leq r \quad (3)$$

Inequalities (1) and (2) determine whether point \vec{q} lies between the two circular faces of the cylinder and inequality (3) determines whether the point lies within the curved surface of the cylinder. We define the set $A_{cyl,j}$ to be the set of clusters assigned to electrode j . Labels were assigned to each cluster in $A_{cyl,j}$ based on the proximity of the cluster centroid to the innermost labeled contact given by the user for each electrode j .

Process Abnormal Clusters. In most cases, the brain-mask did not fully strip the skull, resulting in clusters near the skull being oversized relative to other clusters, each of which correspond to the contacts along electrodes. These clusters were reduced in size by only including points that fall within a sphere of radius $r = 4$ voxels centered at the outermost labeled contact given by the user. Another abnormality that arose was clusters that appeared to be merged. These clusters tended to be the innermost clusters since these contacts typically had the greatest physical deformation during implantation, resulting in the contacts being spatially closer in the CT image. These “merged clusters” tended to contain twice the amount of voxels as other clusters found, but smaller than the skull clusters. These clusters were separated into two using k -means clustering with parameter $k = 2$. As a heuristic for identifying merged clusters and skull clusters, clusters containing between 50 and 200 voxels were processed as merged clusters and clusters containing more than 200 voxels were processed as skull clusters.

Interpolate Centroids. The previous two processing steps aimed to account for artefacts of using too low of a threshold, which can cause clusters to merge. To correct artefacts of using too high of a threshold, we interpolated centroids between adjacent clusters separated by a large distance, accounting for voxel clouds that were masked out. Since contacts are generally evenly spaced along the electrode axis, to obtain a representative point for potentially masked out clusters, we interpolated evenly spaced points between adjacent clusters that were sufficiently far apart. A gap tolerance g of 13 voxels was used to determine the number of points to be interpolated between adjacent cluster centroids.

The number of points to interpolate between adjacent cluster centroids p_i, p_{i+1} was computed as $\lfloor \frac{1}{g} \|p_{i+1} - p_i\|_2 \rfloor$. These new points were appended to each set $A_{cyl,j}$, constructing the corresponding set $A_{pred,j}$. The final set containing each $A_{pred,j}$ will be denoted A_{pred} .

III. RESULTS

We performed semi-automatic electrode algorithm on three patients. We used the corresponding CT image and brain-mask as well as a list bounding contact coordinates for each patient. Images were fully localized manually and used as the validation data for evaluating the performance of the algorithm. Errors were computed as the Euclidean distance between each manually labeled contact and the cluster centroid with the corresponding label. Across three patients, 30 electrodes (479 contacts) were localized (Figure 2). For patient la04, 113 contacts were segmented with a Euclidean distance error of 0.2973 ± 0.2340 mm. For patient la05, 186 contacts were segmented with a mean Euclidean distance error of 0.4927 ± 0.7384 mm. For patient la12, 180 contacts were segmented with a mean Euclidean distance error of 0.4174 ± 0.5899 mm (Figure 3).

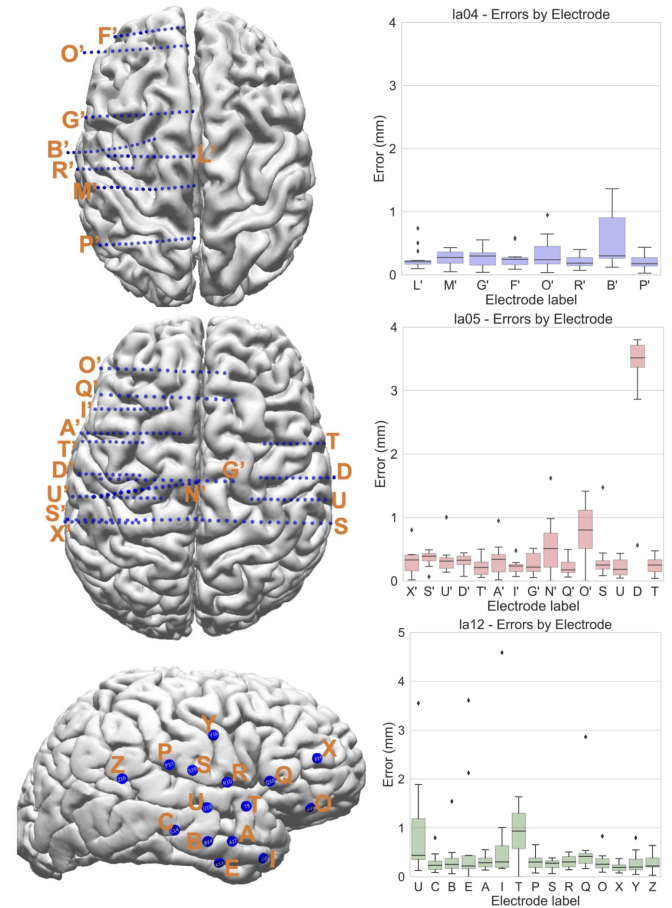


Fig. 2. Examples of localized electrodes in the brain. The left column shows three-dimensional reconstructions from FreeSurfer used by clinicians for pre-implantation planning for each of the three patients in this cohort – la04, la05, and la12 ordered from top to bottom. The right column shows the respective Euclidean distance errors of the predicted centroids against the manually labeled contact coordinates.

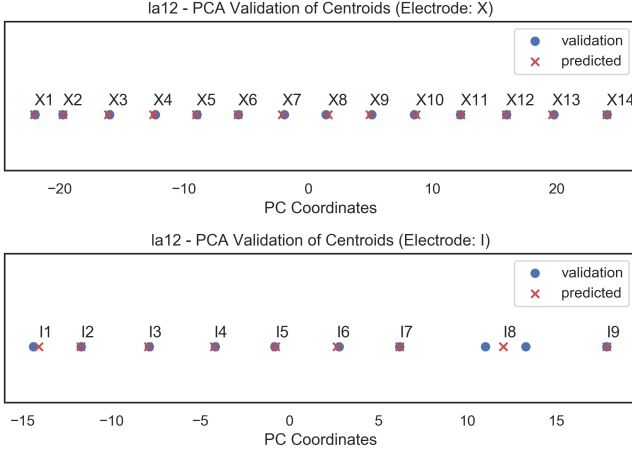


Fig. 3. Error metric for two electrodes of patient la12. The figure overlays the positions of the centroids predicted by the algorithm (red crosses) on the positions of the manually labeled contacts (blue dots) along the principal component with the largest singular value, which should correspond to the electrode axis. The top image pictures the standard localization performed by the algorithm while the bottom image shows an error when interpolating centroids, failing to add an additional point between the centroids labeled I7 and I9.

IV. DISCUSSION

The task of manual localization and neuroanatomical labeling of SEEG contacts is a tedious and error-prone process that consumes several hours of working time of trained clinicians and with significant detrimental consequences if not performed correctly. At the same time, this continues to be the widely used method for localization and labeling of SEEG electrodes with few standardized tools to automate the process. In this study, we examine a threshold-based clustering approach to segmenting and localizing SEEG electrodes in brain scans. Although we utilized a brain-mask in this study derived from T1 MRI, we conjecture that utilizing an automated skull-stripping technique on the CT image would suffice in future studies. In our preliminary study on three patients, we showed the localization algorithm achieves an average error of less than 0.5 mm with only the bounding contact coordinates for each electrode. The semi-automatic localization process was performed within one minute for each patient and provides a fast, robust anatomical labeling that would otherwise require the time of trained experts. While this study exclusively utilized CT images, we can use any type of brain scan (e.g. T1-weighted MRI, T2-weighted MRI) so long as the image has a corresponding brain-mask to strip the skull. Future work will entail segmenting images for a larger cohort of patients, reducing the amount of input from users, and evaluating the performance of a suite of different approaches to robustly localize and label invasive SEEG implantations in epilepsy patients.

ACKNOWLEDGMENT

AL is supported by the NSF GRFP, Whitaker Fellowship and the Chateaubriand Fellowship. SVS is supported by NIH R21 NS103113. Computational resources were also provided by the Maryland Advanced Research Computing Center.

REFERENCES

- [1] Patrick Kwan and Martin J. Brodie. Early Identification of Refractory Epilepsy. *N. Engl. J. Med.*, 342(5):314–319, feb 2000.
- [2] Anne T Berg. Identification of Pharmacoresistant Epilepsy. *Neurol Clin*, 27(4):1003–1013, 2009.
- [3] Anne T. Berg and Molly M. Kelly. Defining Intractability: Comparisons among Published Definitions. *Epilepsia*, 47(2):431–436, feb 2006.
- [4] M. J. Brodie, S. D. Shorvon, R. Canger, P. Halasz, S. Johannessen, P. Thompson, H. G. Wieser, and P. Wolf. Commission on European Affairs: Appropriate Standards of Epilepsy Care Across Europe. *Epilepsia*, 38(11):1245–1250, nov 1997.
- [5] Yong Hua Li, Xiao Lai Ye, Qiang Qiang Liu, Jun Wei Mao, Pei Ji Liang, Ji Wen Xu, and Pu Ming Zhang. Localization of epileptogenic zone based on graph analysis of stereo-EEG. *Epilepsy Res.*, 128:149–157, dec 2016.
- [6] Gabriele Arnulfo, Massimo Narizzano, Francesco Cardinale, Marco Massimo Fato, and Jaakko Matias Palva. Automatic segmentation of deep intracerebral electrodes in computed tomography scans. *BMC Bioinformatics*, 16(1), mar 2015.
- [7] Chuanzuo Yang, Guoming Luan, Qian Wang, Zhao Liu, Feng Zhai, and Qingyun Wang. Localization of Epileptogenic Zone With the Correction of Pathological Networks. *Front. Neurol.*, 9, mar 2018.
- [8] F. Rosenow. Presurgical evaluation of epilepsy. *Brain*, 124(9):1683–1700, sep 2001.
- [9] Liberty S. Hamilton, David L. Chang, Morgan B. Lee, and Edward F. Chang. Semi-automated anatomical labeling and inter-subject warping of high-density intracranial recording electrodes in electrocorticography. *Front. Neuroinform.*, 11, oct 2017.
- [10] Yinghua Wang, Jiaqing Yan, Jianbin Wen, Tao Yu, Xiaoli Li, Hidetoshi Ikeda, and Pierre Mégevand. An Intracranial Electroencephalography (iEEG) Brain Function Mapping Tool with an Application to Epilepsy Surgery Evaluation) An Intracranial Electroencephalography (iEEG) Brain Function Mapping Tool with an Application to Epilepsy Surgery Evaluation. 2016.
- [11] Alejandro O. Blenkmann, Holly N. Phillips, Juan P. Princich, James B. Rowe, Tristan A. Bekinschtein, Carlos H. Muravchik, and Silvia Kochen. iElectrodes: A Comprehensive Open-Source Toolbox for Depth and Subdural Grid Electrode Localization. *Front. Neuroinform.*, 11, mar 2017.
- [12] Juan Pablo Princich, Demian Wassermann, Facundo Latini, Silvia Oddo, Alejandro Omar Blenkmann, Gustavo Seifer, and Silvia Kochen. Rapid and efficient localization of depth electrodes and cortical labeling using free and open source medical software in epilepsy surgery candidates. *Front. Neurosci.*, 7, 2013.
- [13] Chaoyi Qin, Zheng Tan, Yali Pan, Yanyan Li, Lin Wang, Liankun Ren, Wenjing Zhou, and Liang Wang. Automatic and Precise Localization and Cortical Labeling of Subdural and Depth Intracranial Electrodes. *Front. Neuroinform.*, 11, feb 2017.
- [14] Andrew I Yang, Xiuyuan Wang, Werner K Doyle, Eric Halgren, Chad Carlson, Thomas L Belcher, Sydney S Cash, Orrin Devinsky, and Thomas Thesen. Localization of dense intracranial electrode arrays using magnetic resonance imaging HHS Public Access. *Neuroimage*, 63(1):157–165, 2012.
- [15] Michael S. Trotta, John Coejin, Emily Whitehead, Srikanth Damra, John H. Wittig, Ziad S. Saad, Sara K. Inati, and Kareem A. Zaghloul. Surface based electrode localization and standardized regions of interest for intracranial EEG. *Hum. Brain Mapp.*, 39(2):709–721, feb 2018.
- [16] B. Fischl. Automatically Parcellating the Human Cerebral Cortex. *Cereb. Cortex*, 14(1):11–22, jan 2004.
- [17] Mark Jenkinson and Stephen Smith. A global optimisation method for robust affine registration of brain images. *Med. Image Anal.*, 5(2):143–156, jun 2001.
- [18] Robert Oostenveld, Pascal Fries, Eric Maris, and Jan Mathijs Schoffelen. FieldTrip: Open source software for advanced analysis of MEG, EEG, and invasive electrophysiological data. *Comput. Intell. Neurosci.*, 2011, 2011.